Faraday Discussions

Accepted Manuscript

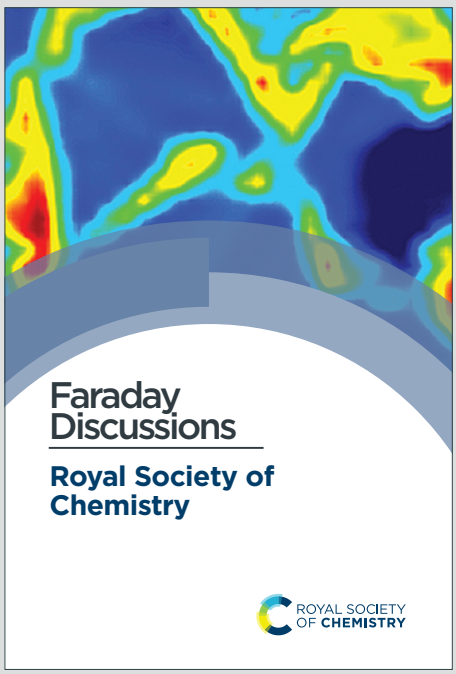

This article can be cited before page numbers have been issued, to do this please use: S. Palakurthy, M. Elbaum and R. Elbaum, *Faraday Discuss.*, 2024, DOI: 10.1039/D5FD00011D.

ROYAL SOCIETY OF CHEMISTRY

www.rsc.org/faraday_d

Silica biomineralization in plants alters the structure of lignin

View Article Online
DOI: 10.1039/D5FD00011D

Srinath Palakurthy[1], Michael Elbaum[2], and Rivka Elbaum[1*]

[1]*The Robert H. Smith Institute of Plant Sciences and Genetics in Agriculture, The Hebrew University of Jerusalem, 7610001 Rehovot, Israel*

[2]*Weizmann Institute of Science, 7610001 Rehovot, Israel*

Abstract

Biomineralization of silica is a major process in plants, which may contribute 3-10% of tissue dry weight. For reasons that remain unclear, plants containing silica are less sensitive to abiotic and biotic stress. In particular, the mechanisms of silica deposition and stress amelioration are still not fully understood. Silica resides mostly in the extracellular volume (the apoplast) which is made of the lignocellulosic cell wall. In a previous work we showed that synthetic lignin catalyses the formation of silica nanoparticles at RC-OSi$(OH)_3$ positions. Since the phenolic O-4 position is the most reactive during lignin polymerization, the binding sites form on the expense of β-O-4 lignin backbone bonds. Therefore, synthetic lignin becomes more branched when polymerized in the presence of silicic acid, as compared to lignin polymerized without silicic acid. To study lignin-silica relationships in the plant, we extracted lignin from stems of wild type sorghum and compared it to lignin extracted from mutants exhibiting high and low silica contents. The thermal stability of both non-extracted biomass and extracted lignin was measured by Thermogravimetric Analysis (TGA). High-silica biomass was thermally less stable than low-silica biomass, suggesting lower content of ether (β-O-4) linkages. This interpretation was supported by Gas Chromatography-Mass Spectroscopy (GC-MS). Fourier Transform Infrared (FTIR) and X-ray photoelectron spectra (XPS) indicated lignin with C-O-Si modifications in all genotypes and further showed silicic acid binding to lignin phenolics and carbonyl moieties. Our results show that lignin extracted from genotypes with native-silicon levels have higher affinity to silicic acid, catalysing silica deposition through Si-O-4

(Si-phenoxyl) bonds and suggest that the presence of silicic acid during *in vivo* lignin polymerization reduces β-O-4 ether linkages.

View Article Online
DOI: 10.1039/D5FD00011D

Key words: Plants, Biomineralization, Lignin, Silica.

1. Introduction

View Article Online
DOI: 10.1039/D5FD00011D

Biomineralization, the process by which organisms produce minerals, is indeed found in a wide variety of organisms, including plants, fungi, bacteria, and animals. The self-amplifying nature of biomineralization is particularly fascinating, as it involves a feedback loop in which small initial mineral particles or structures gradually grow into larger and more complex structural supports (e.g., shells, skeletons, bone and teeth). This synergistic response helps organisms to maximize their survival, contributing to both growth and survival in a dynamic and changing environment. Mineral formation by organisms is usually carried out in an aqueous environment at atmospheric pressure and temperature, and involves organic biomacromolecules that self-organize into highly ordered structures under regulation of the organisms. These macromolecules act as templates that control the morphology and molecular/atomic structure of mineralised phases. These hybrid structures of organic and inorganic materials have unique functions not seen in single-component materials. Therefore, understanding the biomineralization process can promote novel methods for the production of green functional materials to meet the needs of modern society [1–3].

Plants growing in silica-rich soil take up soluble silicic acid from the soil solution and transform it into solid amorphous silica. Silicic acid moves with water in the extracellular space, called the apoplast, which is made of lignocellulosic cell walls and voids. With the help of the transpiration stream and dedicated protein transporters [4], silicic acid is distributed in the plant body and gets deposited mostly at the epidermis of leaves and stems (Fig. 1) [5]. The organic environment of cell walls, including abundant proteins, polysaccharides (cellulose and hemicellulose), and phenolic (lignin) compounds, is likely to play an ultimate role in the formation of silica [6]. A few reports suggest that silicon (Si, as silicic acid or silica) affects the composition of plant cell walls *in vivo* [7–9] and *in vitro*, by binding to phenolic components in polymerization reactions [10]. Reciprocally, silica formation was linked with lignin formation *in*

View Article Online
DOI: 10.1039/D5FD00011D

vitro [11–13] and *in vivo* [14,15]. However, molecular details explaining lignin-assisted biosilicification in plants are only fragmentary.

Simplified *in vitro* system of peroxidase-catalyzed polymerization of lignin model compound shows that silica is precipitated by polymerizing lignin, but not by lignin monomers, and that silica prevents the formation of large lignin fragments [10,11]. We have shown that silicic acid binding at the phenoxyl radical/quinone methide moieties of lignin reduces alkyl-aryl ether (β-O-4) backbone linkages in the final lignin. Synthetic lignin catalyses silica deposition through covalent Si-O-C bonding, which lead to the growth of 2-5 nm silica particles [16].

In plants, lignin is secreted into a cellulose - hemicellulose structure in secondary cell walls. Pure lignin typically accounts for 15-30% of lignocellulosic biomass. It is covalently linked to hemicellulose, usually by ester bonding, and thereby crosslinks polysaccharides, providing mechanical strength and rigidity to the cell wall (Fig. 1) [17–19]. Delignification, the process of extracting lignin during pulping pretreatment procedures, disrupts the glycosidic bonds in polysaccharides. As a result, hydrolysable linkages in lignin may break as well [20]. Lignocellulosic biorefinery technologies have developed a process using acetic and formic acid-based organosolv fractionation of lignin from biomass without degradation or extensive modification [21,22]. This method adds carboxylic acid groups to extracted lignin molecules through esterification (acetate and formate) that are cleavable upon hydrolysis [23,24].

Sorghum is a highly productive grain staple crop, tolerant to drought and salinity [25]. The high silicon accumulation in sorghum may interfere with its dual role as food and fodder/biofuel source [26]. Sorghum biomass is also a research target for developing second-generation biofuels that do not compete with food production [27]. Further, sorghum is a model plant for studying silica deposition [28]. As such, a sorghum mutant carrying a defective gene for

View Article Online
DOI: 10.1039/D5FD00011D

silicon root transporter- *Sblsi1*, was isolated, which absorbs about 200 times less silica as compared to the wild type (WT) plant [29].

In the present work, *in planta* lignin-silica relationship was studied by analysing the lignin of native- and low-silicon (*Sblsi1*) sorghum genotypes. We compare the effects of Si uptake in the background of both wild type (WT) and a lignin mutant presenting extra aldehyde on the expense of hydroxyl lignin groups (brown mid-rib 6, *bmr6* [30]). The pyrolysis behaviour of unextracted biomass and of acid-based organosolv isolated lignin indicated a higher content of native aryl-alkyl ether (β-O-4) linkages in low-silicon genotypes. Lignin extracted from high silicon genotypes had higher catalytic activity in silicic acid polymerization, as compared to lignin extracted from low-silicon genotypes. We identified Si-O-C bonds that formed during lignin synthesis *in planta* and suggest that these positions catalyse formation of SiO_2 nanoparticles.

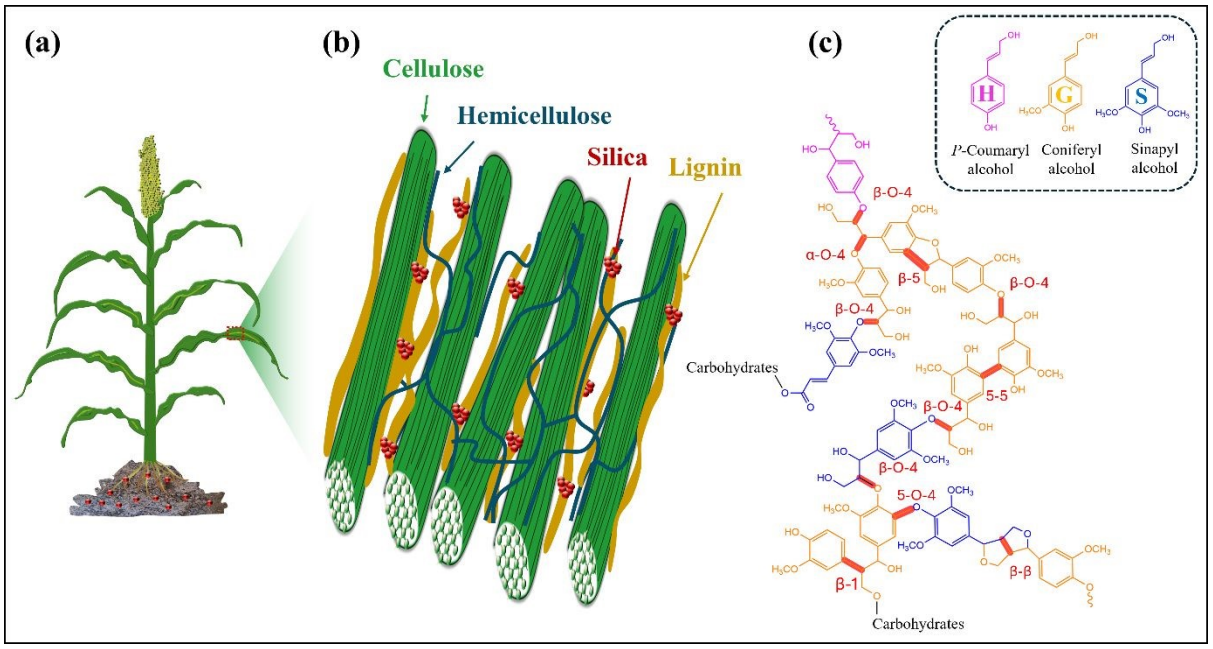

Figure 1: Cell wall model, demonstrating silica deposited into the cell wall matrix. (a) sorghum plant planted in silicate (red) soil which contains silicic acid available for root intake. The bulk of silicic acid resides in the apoplast, i.e. the extracellular space, and moves with the

View Article Online
DOI: 10.1039/D5FD00011D

water transpiration stream to the shoot. (b) silica deposits (red) in the cell wall, onto a lignin (orange) – hemicellulose (blue) matrix that binds cellulose microfibrils (green). (c) lignin model structure, made of three canonical monomer units, H, G, and S, bound via β-O-4 backbone connection and other phenylpropanoids via a random radical-driven dehydrogenation. β-O-4 are the most abundant linkages in natural lignins [31].

2. Materials and methods

2.1 Materials and reagents

Formic acid (FA, reagent grade, ≥95%, Sigma Aldrich) and glacial acetic acid (AA, Reagent Plus, ≥99%, Sigma Aldrich) were used in lignin extractions. Dipotassium hydrogen orthophosphate (K_2HPO_4) and potassium dihydrogen phosphate (KH_2PO_4) were used to prepare 0.1 M potassium phosphate buffer solution at pH 7.4. 1 M silicic acid was produced by adding 150 µL tetramethyl orthosilicate (TMOS, Sigma-Aldrich) to 850 µL 1 mM hydrochloric acid (HCl, ACS reagent, 37%, Sigma Aldrich), and mixing for 30 min. Boron trifluoride diethyl etherate (>46.5% BF_3, Sigma Aldrich), ethanethiol (99+%, thermo scientific), 1, 4-dioxane (99.8%, Sigma Aldrich), bisphenol-A (≥99%, Sigma Aldrich), sodium bicarbonate ($NaHCO_3$, 99.5%, Merck), and ethyl acetate (99.9%, Sigma Aldrich) were used in thioacidolysis.

2.2 Plant materials

Sorghum bicolor (L.) Moench, line BTx623 (wild type, WT), low-silicon mutant (*Sblsi1*), with about 1:200 content of silica in relation to WT plants [29], and brown midrib (*bmr6*) containing altered lignin composition [30] were grown in green house. In addition, we produced a cross between *bmr6* and *Sblsil* (*bmr6*×*lsi1*), F1 hybrid, and propagated it via self-fertilization to F2 inbred lines. Selection for F2 line carrying both *bmr6* and *Sblsi1* mutations was done based on

View Article Online
DOI: 10.1039/D5FD00011D

PCR amplification of the mutated genes (Supplementary Information SI1). Plants mutated at both *Sblsi1* and *bmr6* were grown in parallel to the other genotypes. No visual variation in growing parameters was detected between the four genotypes. Stems of approximately 3-month-old plants were collected, physically cut into less than half-centimetre pieces, and thoroughly washed under running tap water and then distilled water. The washed pulp was dried in an oven at 70°C for 3 days. The final dried samples were stored for later use.

2.3 Determination of silica content in biomass

Approximately 2 grams of chopped and dried sorghum stems were placed in muffle furnace using porcelain crucibles and heated at 600°C for 12 h. The ash was collected and treated with 1 M HCl and washed once with distilled water. The final acid insoluble ash (AIA) was weighed, AIA was considered to be mainly silica, and its percent per dry weight biomass was calculated [32].

2.4 Isolation of lignin

The lignin fraction was extracted by mixing 1 g (dry matter) of chopped sorghum stems in a volume of 10 mL acetic acid/formic acid/water medium (AA/FA/H_2O: 55/30/15 volume ratio) [22]. It was pre-soaked for 30 min at 50°C on a heating plate. After soaking, the mixture was kept at 100°C for 2.5 h with continuous stirring. The mixture was allowed to cool down to room temperature and then filtered with a vacuum filter funnel assembled with a filter disk (11 µm pore size; Whatman filter paper). Acids were evaporated from the filtrate fraction containing the extract liquor until reaching around 60% dry matter volume by vacuum evaporation (320 mbar). Distilled water was added to the concentrated extract liquors while stirring, to increase the solution pH from a baseline value below 1 to precipitate the lignin at around pH 2. We noted that the water/concentrated liquor ratio to achieve optimal lignin precipitation was 2/1 for WT and *bmr6* and 4/1 for *lsi1* and *bmr6*×*lsi1*. The precipitates were recovered by

centrifugation and washing once with phosphate buffer (pH 7.4) and two times with distilled water.

View Article Online
DOI: 10.1039/D5FD00011D

2.5 Lignin-silicic acid precipitation process

Isolated never-dried lignin particles (approximately equal to the dried weight of 3 mg) were dispersed in 3.8 mL of 0.1 M phosphate buffer solution at pH 7.4. Silicic acid at concentrations of 2.5 and 5 mM was added to the solution agitated at 200 rpm for 3 days in the dark. Samples were centrifuged at 9000 rpm and the precipitate was washed 3 times with double distilled water, and dried under vacuum at room temperature.

2.6 Characterization

Thermogravimetry analysis (TGA)

About 10 mg of sample (of dried biomass or isolated lignin samples that were dried under vacuum in a desiccator) was placed in platinum crucibles and linearly heated from ambient room temperature to 900°C at a rate of 10°C/min in a thermogravimetry analyser (TGA-Q500 series, TA instruments). Nitrogen gas at a flow rate of 90 mL/min was used to purge the system and also provided an inert atmosphere for the experiments.

Gas chromatography-mass spectrometry (GC-MS)

Thioacidolysis reaction was performed according to a previously published procedure [33]. The plant materials were grounded into powder in liquid nitrogen and then vacuum dried overnight. 2 mg of dry ground biomass were accurately weighed into a 2 mL Teflon-lined screw-cap micro-reaction vessel. Thioacidolysis reagent was prepared by mixing 2.5% boron trifluoride diethyl etherate, 10% ethanethiol and 87.5% dioxane by volume. Bisphenol-A was added as an internal standard at a concentration of 0.05 mg/mL. One mL of thioacidolysis reagent was added to each vial containing the biomass and the vials were tightly capped. The reaction was

View Article Online
DOI: 10.1039/D5FD00011D

run at 100°C for 4 h, quenched by cooling on ice for 5 min, and vortexed. The insoluble residue was allowed to settle, and 400 µL of the supernatant was transferred into 4 mL glass vials. 250 µL of 1 M aqueous sodium bicarbonate solution, 125 µL of 2 N HCl, 1000 µL double distilled water, and 500 µL ethyl acetate were added sequentially and the samples were vortexed to ensure mixing. The oily organic layer obtained was subjected to GC-MS analysis (GCMS-350). The trimethylsilyl derivatives of lignin monomers were identified and quantified relative to the internal standard.

Fourier transform infrared (FTIR) spectroscopy

Isolated lignin and lignin-silicic acid samples were dried under vacuum in a desiccator. Analysed pellets were prepared by mixing ~1 mg of dry powdered samples with ~99 mg of KBr. Fourier transform infrared (FTIR) spectra were obtained in transmittance mode using a Nicolet 6700 FT-IR spectrometer (Thermo Fisher Scientific, Inc), with 20 spectral scans in the range from 400 to 4000 cm^{-1} with a resolution of 4 cm^{-1}. Peak fitting analysis was performed on the FTIR absorption spectra using Lorentz peak fitting, with absorbance calculated as a logarithmic function of transmittance (absorbance = 2 - log10 (% T)). The relative change in the integrated absorption area of the deconvoluted absorption bands was calculated as the difference between the normalized (peak area/total area of fitted range) peak area.

X-ray photoelectron spectroscopy (XPS)

X-ray photoelectron spectroscopy (XPS) measurements were performed on a K-alpha XPS system (Kratos, Kratos Analytical Ltd.) using high-resolution monochromatic Al Kα X-ray as the excitation source. Isolated lignin and lignin-silicic acid samples were dried under vacuum in a desiccator. Dry samples were excited by Al Kα X-rays (hν = 1486.7 eV) with a working voltage of 15 kV and an emission current of 40 mA. Multiplex (narrow) high-resolution spectra

of the C1s, O1s and Si2p regions were collected. The spectra were analysed using built-in Kratos software.

View Article Online
DOI: 10.1039/D5FD00011D

Scanning electron microscopy-energy-dispersive X-ray spectroscopy (SEM-EDS)

The structural morphology and elemental composition were studied using a high-resolution scanning electron microscope (HR-SEM, JSM-7800f) jointly equipped with energy-dispersive X-ray spectroscopy (EDS). A drop of ~5 µL of isolated lignin and lignin-silicic acid precipitates were drawn, deposited onto carbon tape mounted on an aluminium stub, and then dried at room temperature. Images of dry samples were collected using a secondary electron detector on AuPd sputter-coated samples with 2.00 kV beam energy and 4.00 mm working distance.

Scanning transmission electron tomography and EDS

Specimens were prepared on 200 mesh Cu C-flat grids (Protochips, USA) by drop-casting 5 µl of the material suspended in deionized water, followed by gentle air-drying. The electron microscope, a Tecnai T20-F (FEI Inc, USA), was operated at 200 kV acceleration in the STEM microprobe mode with a 30 micron C2 aperture (for 0.8 mrad semi-convergence angle). The detector was an ARINA (DECTRIS SA, Switzerland) hybrid pixel camera, operated in parallel with the standard high angle annular dark field detector, both controlled by a custom scan generator [34]. Camera length was 100 mm and pixel size 1.54 nm. Probe current was 10 µA and 6.5 µA for the *bmr6* and *bmr6×lsi1* samples, respectively. While samples were prepared and dried at room temperature, tomography was performed under cryogenic conditions in order to suppress carbon contamination in the microscope vacuum. Low-dose protocols were followed in order to avoid warping and distortion of the lignin assemblies. Tomographic series were recorded in dose-symmetric mode covering the range of -60 to 60 deg in 3 deg steps and aligned by patch tracking in IMOD [35]. A signal representing the integration of the central disk projected

View Article Online
DOI: 10.1039/D5FD00011D

to the camera, i.e., the incoherent bright field image, was reconstructed by SIRT with 100 cycles using tomo3d [35]. Contrast was inverted in preparation of figure 10, with mapping of dark values to partial transparency so as to reveal the strongly scattering nanoparticles embedded within the lignin matrix.

Energy-dispersive X-ray spectroscopy measurements were acquired in a Talos 200-X microscope (Thermo-Fisher Scientific) equipped with a QUANTAX FlatQUAD spectrometer (Bruker). As above, the measurements were performed under cryogenic conditions. Data were analysed using the embedded Velox software.

3. Results and discussion

3.1 Variations in biomass composition of four sorghum genotypes

To understand the effect of silicic acid and silica on lignin structures, we grew sorghum wild type (WT) plants, mutants in lignin biosynthesis (*brown midrib 6, bmr6* [30]), and mutants in silicic acid intake (low silicon 1, *lsi1* [29]). We also produced double mutant plants by crossing a mutant in *bmr6* with a mutant in *lsi1* (*bmr6*x*lsi1*, see SI1 for details). Silica content was measured in the stems (Table 1). As expected, much lower percentage of silica was observed in the biomass of both low-silicon genotypes (*lsi1* and *bmr6*x*lsi1*, herein BM-LowSi) as compared to genotype with native-silicon intake (WT and *bmr6*, herein BM-HighSi). Furthermore, a slightly higher percentage of silica was observed in both lignin mutants (*bmr6* and *bmr6*x*lsi1*), in accordance with published results [15].

Table 1: Fractionation of sorghum stems into silica and organic phases. Percentage silica per biomass dry weight was measured by weighing the acid insoluble ash (AIA). Percent weight per biomass or per isolated lignin dry weight are calculated based on Thermal gravimetric

View Article Online
DOI: 10.1039/D5FD00011D

analysis (TGA) (Fig. 2). Stage i represented residual water loss, Stage ii represented polysaccharides decomposition and lignin interunit linkages and side chain breaking, Stage iii (Biomass) or Residue (Lignin) represented lignin carbonization.

Sorghum genotype	**Silica (% weight per biomass dry weight)**	**Thermal gravimetric analysis (TGA)**									
		Biomass						**Lignin**			
		Stage-i (40-170ºC)		Stage-ii (170-480ºC)		Stage-iii (480-900ºC)		Stage-ii (170-480ºC)			Residue (%)
		Weight loss (%)	Peak (°C)	Weight loss (%)	Peak (°C)	Weight loss (%)	Peak (°C)	Weight loss (%)	Peak 1 (°C)	Peak 2 (°C)	
WT	2.0±0.2	3.4	154	56.7	316	21.1	~600	55.2	256	353	23.3
lsi1	0.04±0.02	5.8	160	59.9	343	10.7	~600	57.5	269	363	28.1
bmr6	2.3±0.2	5.6	154	55.7	320	11.8	~600	57.2	254	338	23.3
bmr6×lsi1	0.3±0.1	8.7	154	53.2	331	8.5	~600	59.2	263	342	25.8

Thermal gravimetric analysis (TGA) of stems from flowering plants presented a three-stage decomposition process, with distinct weight loss rates, as seen by differential thermal gravimetry (DTG), (Fig. 2ab and Table 1): (i) moisture loss (40-170°C); (ii) lignin rapid devolatilization (170-480°C) and polysaccharide decomposition (220-480°C) including hemicellulose (220-310°C) and cellulose (300-480°C); and (iii) char formation (>480°C), where the carbonaceous lignin reduced to graphite [36]. A shift of the polysaccharide decomposition (stage ii) to higher temperatures was detected in the BM-LowSi as compared to BM-HighSi (Table 1). This could indicate increased crosslinking in the low-silicon cell walls, pointing to changes in lignin structure (See Fig. 1) [37]. Furthermore, the mass which was lost during char formation (stage iii, > 480°C) was lower in BM-LowSi as compared to BM-HighSi (Table 1). This could result from a possible role of silica in facilitating reduction and evaporation of lignin radicals [16].

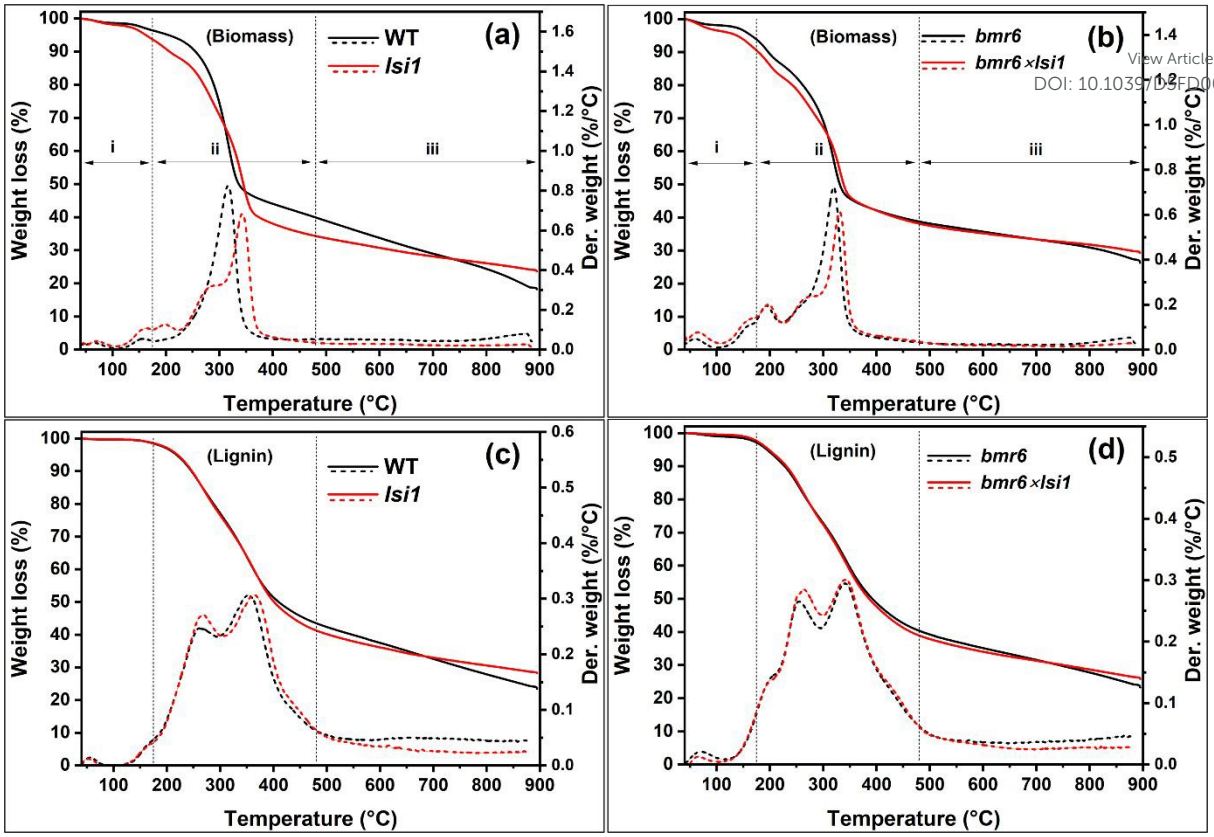

Figure 2: Thermal decomposition of biomass (a,b) and isolated lignin (c,d) from stems of four sorghum genotypes. Biomass thermal degradation (continuous lines) and degradation rates (dotted lines) of (a) WT (black) compared to low silicon *lsi1* (red), and (b) lignin mutant *bmr6* (black) compared to low silicon lignin mutant *bmr6×lsi1* (red). Thermal degradation and degradation rates of lignin extracted from stems of (c) WT (black) and *lsi1* (red), and (d) *bmr6* (black) and *bmr6×lsi1* (red). Degradation was divided to stages i, ii, iii, and % weight of each stage was calculated (Table 1).

To further confirm the increase in crosslinking and other possible changes in lignin structure in BM-LowSi (herein Lig-LowSi) in comparison to lignin in BM-HighSi (herein Lig-HighSi), lignin monomers were isolated via thioacidolysis of the biomass, and β-O-4 cleavage derived monomers were quantified by GC/MS (Fig. S1). Thioacidolysis relies on the selective cleavage of β-O-4 ether linkages to produce thioethylated H, G and S monomers (see inset of

Fig. 3) [38,39]. G and S-derived monomers were the major products in all genotypes, while H-derived monomers were detected at trace levels. The yield of monomers and S/G ratio derived from lignin mutants *bmr6* and *bmr6×lsi1* were lower compared to WT and *lsi1* genotypes (Fig. 3), in agreement with published analyses of lignin composition in the *bmr6* sorghum genotype [30]. All three monomer yields obtained from BM-LowSi were higher than those obtained from BM-HighSi, similarly to published data [9]. This could be interpreted as an increase in the lignin fraction in the BM-LowSi relative to BM-HighSi. However, our TGA results do not show such trends (Fig. 2ab, Table 1). Therefore, we relate this variation simply to increased β-O-4 linkages in the BM-LowSi as compared to BM-HighSi, similarly to synthetic lignin produced *in vitro* [16].

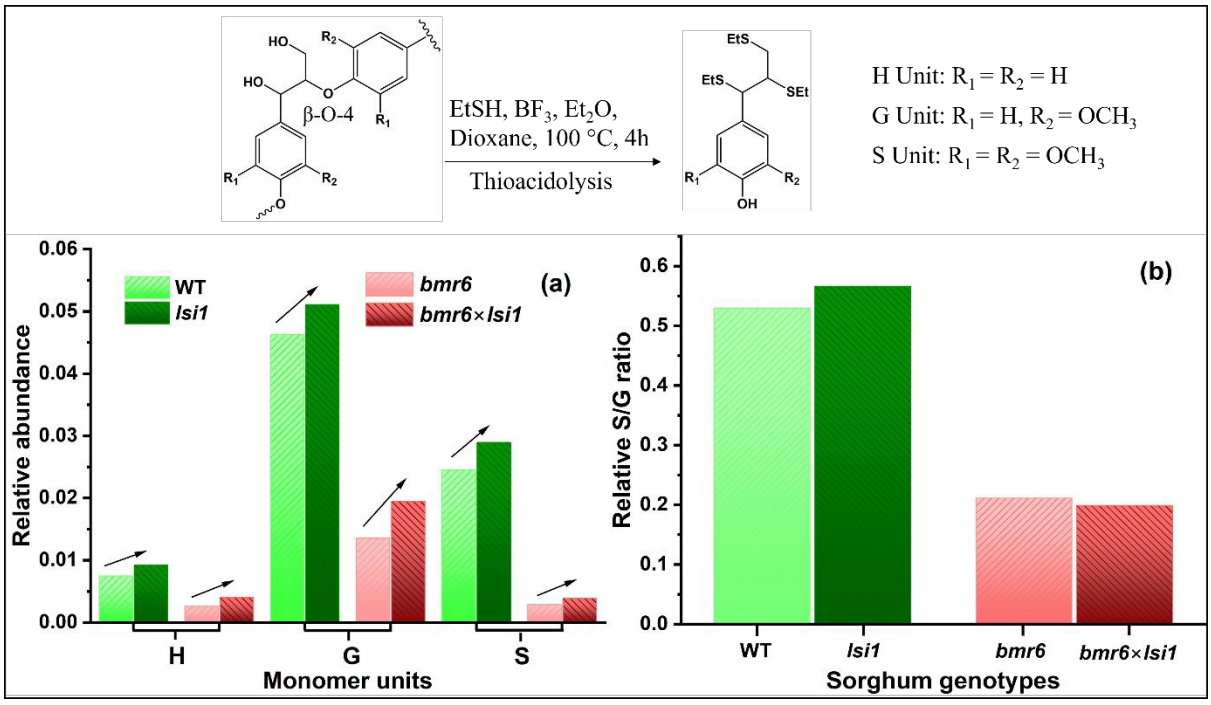

Figure 3: Distribution of major lignin units in stems of sorghum genotypes quantified by GC-MS following thioacidolysis. (a) Abundance of monomer units calculated by measuring peak area of ions relative to an internal standard. Arrows demonstrate a trend of increased monomer release in BM-LowSi (dark shadow) as compared to BM-HighSi (light shadow) in native (green) and mutated (red) lignin genotypes. (b) Calculated monomer S/G ratio. Color-

codes are similar to panel a. Inset: representative chemical reaction of the formation of thioethylated H, G and S monomers by the cleavage of β-O-4 ethers in lignin.

View Article Online
DOI: 10.1039/D5FD00011D

3.2 Variation in structure of extracted lignin

To highlight the effects of silicic acid or silica on lignin structure, lignin was isolated from the stems biomass by acid based organosolv extraction. Scanning electron micrographs (SEM) of isolated lignins showed spherical lignin particles of 10 to 50 nm in diameter that aggregated into a porous mesh (Fig. 4). Lignin extracted from *bmr6* mutants (*bmr6* and *bmr6×lsi1*) aggregated into finer mesh, as compared to the lignin extracted from WT and *lsi1* plants, indicating of some variations in the self-assembly of the mutated polymer. The Lig-LowSi formed a more open network, as compared to Lig-HighSi. All lignin samples had residual Si, as detected by energy dispersive X-ray spectroscopy (EDX) elemental analyser. However, the average Si content was higher in Lig-HighSi than in Lig-LowSi (Tables in Fig. 4). Interestingly, the fraction of oxygen was higher, and carbon was lower, in Lig-HighSi as compared to Lig-LowSi, suggesting that the functional groups were more oxidized in Lig-HighSi than in Lig-LowSi.

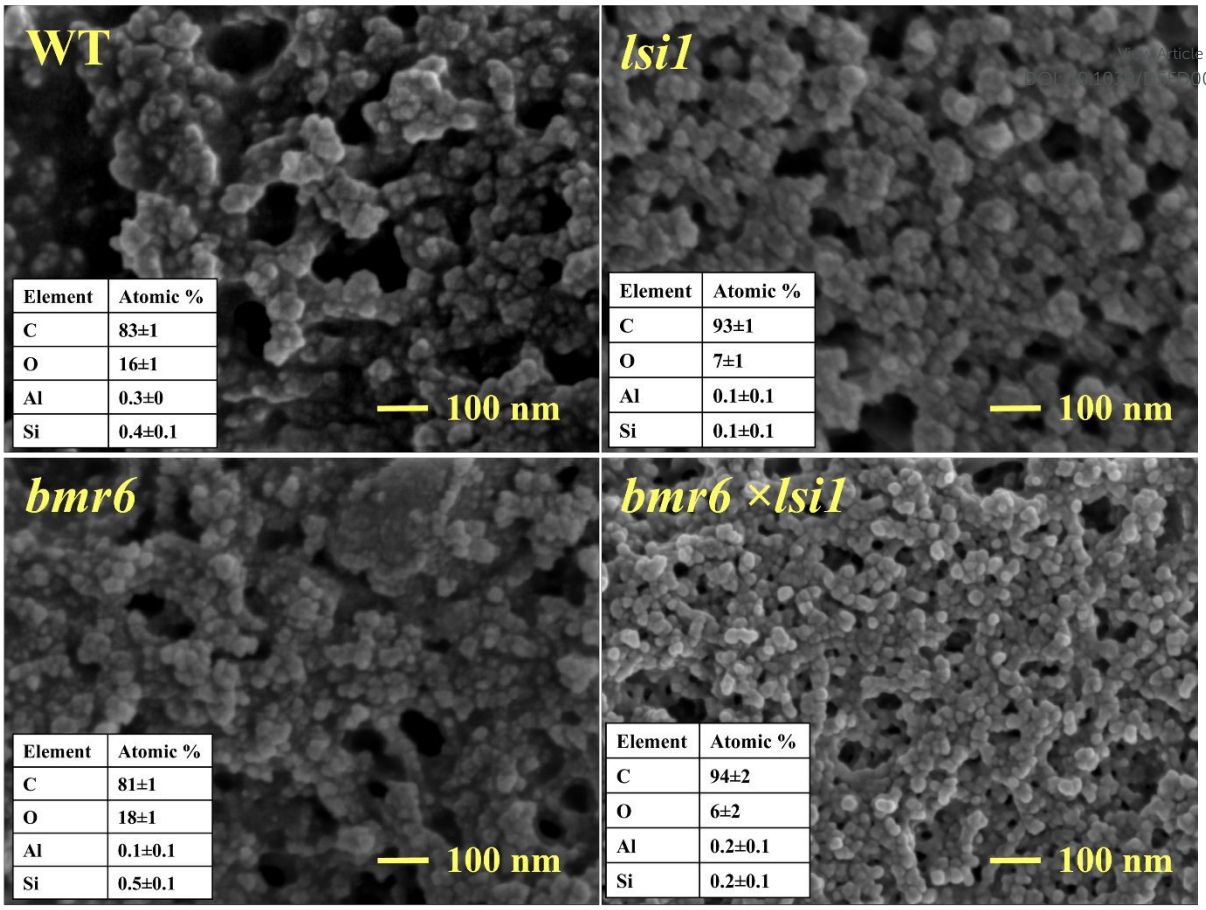

Figure 4: Scanning electron micrographs of lignin extracted from four sorghum genotypes, as marked on the images. Insets: tabulated mean element content ± standard deviations of at least five EDX spectral measurements.

Pyrolysis of the extracted lignin occurred over a wide temperature range, from about 200°C to 800°C, with fast weight loss rate in parallel to the polysaccharide decomposition (stage ii, 170-480°C) (Fig. 2cd, Table 1). Stage ii thermal decomposition of the isolated lignin divided to two maxima, at 254-269°C and 338-350°C. The first decomposition peak was associated with cleavage of aryl-alkyl ether (β-O-4) linkages to produce phenols and aromatic hydrocarbons [40,41]. This peak was bigger and shifted to higher temperatures in Lig-LowSi as compared to Lig-HighSi. Possibly, Lig-LowSi contained higher fraction of ether bonds that broke to

View Article Online
DOI: 10.1039/D5FD00011D

produce higher concentration of volatile molecules, as compared to Lig-HighSi. The second peak was attributed to lignin side chain decomposition such as carboxylic acid and carbonyl group cleavage and oxidation, and dehydroxylation and hydroxyl cracking in lignin hydrogen bond network [40,41]. This peak varied in lignin extracted from the different genotypes, possibly indicating variation in the distribution of side chain functional group content.

Fourier transform infrared (FTIR) spectroscopy of the isolated lignins indicated structural differences between the samples. The C=O stretch of conjugated aldehyde carbonyls at 1655 cm^{-1} was more abundant in mutated lignin extracted from *bmr6* and *bmr6×lsi1*, while non conjugated carbonyls of ketone and esters at 1710 cm^{-1} were abundant in lignin extracted from WT and *lsi1*. The intensities of absorptions assigned to S units at 834 cm^{-1} (C-H deformation) and 1330 cm^{-1} (C-O stretch) lower relative to the aromatic skeletal vibration at 1514 cm^{-1} in mutated lignin (*bmr6* and *bmr6×lsi1)* compared to WT and *lsi1* lignin (Fig. 5, Table 2). These results indicate that *bmr6* sorghum mutants have reduced S:G ratio, consistent with GC-MS results (Fig. 3) and the literature showing significantly reduced S-units and production of more aldehyde groups during biosynthesis in *bmr6* sorghum mutants [30,42].

Plant silicon intake also affected lignin FTIR signature. The strong absorption band at 3100-3600 cm^{-1}, attributed to the stretching vibrations of OH groups, was broader for Lig-HighSi as compared to Lig-LowSi (Fig. 5a). This could be attributed to a high concentration of hydroxyl moieties in Lig-HighSi on the expense of β-O-4 linkages, in agreement with TGA and GC-MS (Fig. 2,3). In accordance, the peak at 1168 cm^{-1} was bigger in Lig-LowSi compared to corresponding Lig-HighSi (red arrows in Fig. 5b). This peak could be assigned to conjugated carbonyl moieties (C=O located at α position) and commonly observed in H-G-S type lignin [43,44].

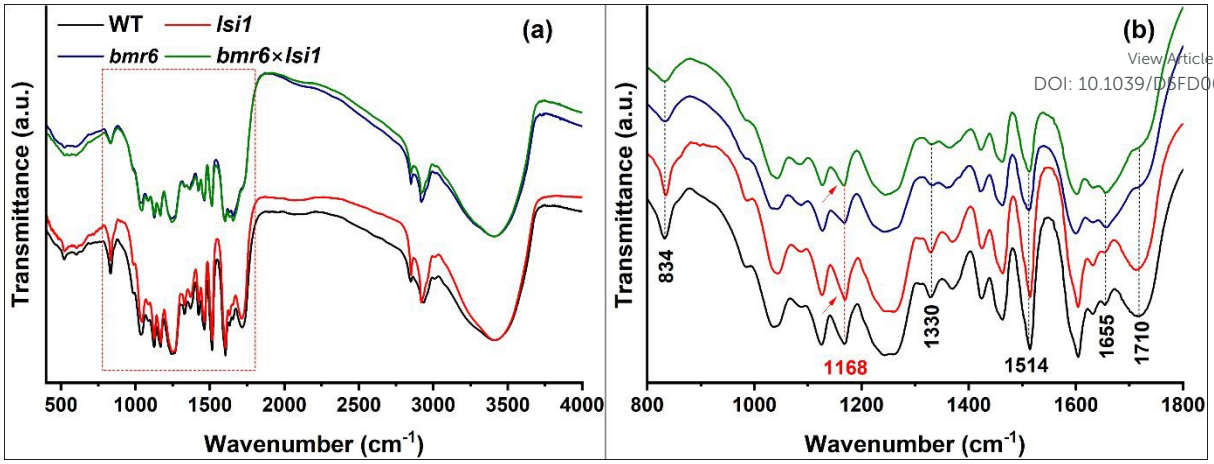

Figure 5: FTIR transmission spectra of isolated lignin. Lignin extracted from wild type (WT, black), *lsi1* mutant (*lsi1*, red), *bmr6* mutant (*bmr6*, blue), and a double mutant in *lsi1* and *bmr6* (*lsi*×*bmr6*, green) sorghum genotypes, showing characteristic functional groups between 400 and 4000 cm^{-1} (a), and between 800 and 1800 cm^{-1} (b), as marked by a rectangle in panel a. Structural differences in lignin, as a result of the *bmr6* mutation are indicated by black vertical dotted lines. Conjugated carbonyl groups associated with silica-lignin interactions as a result of the *lsi1* mutation are indicated by a red vertical dotted line. Arrows indicate an increase in the absorptions of these carbonyls in lignins of low-silicon as compared to native-silicon genotypes. See Table 2 for band assignments.

Table 2: Assignment of infrared absorption bands of lignins, Si-O-C and Si-O-Si bonding vibration modes.

Observed bands (cm^{-1})	**Assignment**	Source
3390-3435	O-H stretching	45,46
3005	C-H stretch of OCH_3	
2935	Symmetric C-H stretch of OCH_3 and antisymmetric stretch of CH_2OH	
2848	Symmetric C-H stretch of OCH_3	
1710	C=O stretch of non-conjugated carbonyls	
1654	C=O stretch of conjugated carbonyls	

1630	O-H bending	
1605	Aromatic ring stretch	
1514	Aromatic ring stretch	
1463	C-H bending of OCH_3 and CH_2	
1423	Aromatic ring stretching with in plane C-H deformation	
1369	Aliphatic C-H stretch in CH_3; not in OCH_3; phenolic OH	
1330	C-O stretch of S ring; ring stretch of asymmetric-tetrasubstituted rings	
1275	C-O stretch of G ring; C=O stretch	
1265	C-O stretch of G ring; C=O stretch	
1240	Si-phenoxy	47
1217	C-C, C-O, C=O stretch; G condensed > G etherified	44–46
1204	C-C stretch	
1168	C=O stretch in ester group of HGS lignin	
1158	Si-O-C asymmetric stretching or C-O-Si cage link structure	47,48
1125	Aromatic C-H deformation of G units	45,46
1116	Si-O-C asymmetric stretching or C-O-Si open link structure	48
1085	C-O deformation in secondary alcohols and aliphatic ethers	45,46
1063	Si-O-C asymmetric stretching or C-O-Si ring link structure	47,48
1050	Si-O-Si asymmetric stretching of open chain siloxanes	
1034	C-O deformation primary alcohols; C-O stretch of methoxy groups	45,46
1015	Si-O-Si asymmetric stretching of cyclic siloxanes	48
986	HC=CH out-of-plane deformation	45,46
975	Si-phenoxy	47
832	C-H bending of S units	45,46
523	Aromatic ring C-H deformation	
469	Si-O-Si bending vibrations	49

XPS of C 1s showed the presence of four species of carbon atoms with distinct binding energies (Fig. 6a). C_1 bond at 285 eV corresponded to non-oxidized carbon (C-H, C-C, C=C); C_2 bonded at 286.5 eV corresponded to carbon bound to one oxygen through a single bond (C-OH, C-O-C); C_3 bonded at 288.2 eV corresponded to carbon bound to oxygen with two bonds (C=O), attributed to carbonyls; and C_4 bonded at 289.2 eV corresponded to carbon with three bonds to oxygen (O-C=O), attributed to ester and carboxylic acid groups [50,51].

Atomic ratio of carbon to oxygen (O/C) quantified by XPS was higher in Lig-HighSi than in Lig-LowSi (Table 3), in agreement with SEM-EDX results (Fig. 4). This may indicate a higher content of phenolic hydroxyls (C-OH) on the expense of β-O-4 ether bonds (C-O-C) in Lig-HighSi relative to Lig-LowSi, in accordance with the FTIR indication of increased hydroxyls in Lig-HighSi relative to Lig-LowSi (Fig. 5a). The lower fraction of C_3 bonds in Lig-HighSi indicates that it may contain less carbonyls (C=O) than Lig-LowSi (Fig. 6a, Table 3). Interestingly, we noted that liquor extracted from BM-HighSi was less acidic than liquor extracted from BM-LowSi (see materials and methods section 2.4). This supports our analysis that Lig-HighSi contains high fraction of phenolic hydroxyl groups (pKa ~ 10) and low fraction of carbonyl groups (pKa ~ 4.4) [52].

Table 3: XPS oxygen to carbon atomic concentration ratio (O/C) and percent of assigned carbon species.

Samples	Percent of carbon species (%)									
	O/C		C_1 (C-C, C-H, C=C)		C_2 (C-O)		C_3 (C=O, O-C-O)		C_4 (O-C=O)	
	0 mM Si	2.5 mM Si	0 mM Si	2.5 mM Si	0 mM Si	2.5 mM Si	0 mM Si	2.5 mM Si	0 mM Si	2.5 mM Si
WT	0.29	0.3	48	48	40	45	9	4	3	4
lsi1	0.24	0.3	42	41	37	49	19	7	2	4
bmr6	0.26	0.3	51	52	40	42	6	3	3	3
bmr6×lsi1	0.22	0.3	53	56	33	37	12	4	2	3

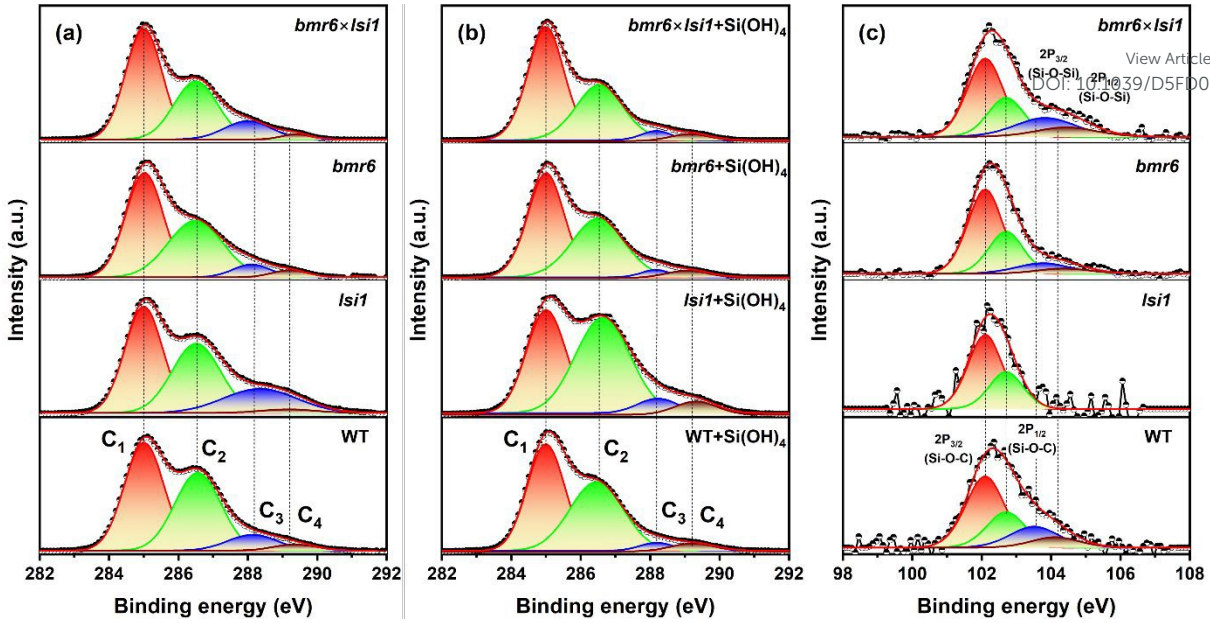

Figure 6: High resolution XPS C 1s and Si 2p spectra of four sorghum genotype lignins and lignin-silicic acid (lignin+Si) precipitates: (a) C 1s spectra of lignin extracted from WT, *lsi1*, *bmr6* and *bmr6×lsi1* sorghum genotypes. Peaks of C_1 (C-C, CH, red), C_2, (C-OH, green) C_3 (O-C-O, C=O, blue), and C_4 (O-C=O, brown) are deconvolved. (b) C 1s spectra of lignin+Si from WT, *lsi1*, *bmr6* and *bmr6×lsi1* sorghum genotypes precipitated with 2.5 mM silicic acid solution. Reduction in C_3 peaks (blue) with addition of silicic acid indicated reduction in C=O groups that possibly reacted to give Si-O-C. (c) Si 2p spectra of lignin extracted from WT, *lsi1*, *bmr6* and *bmr6×lsi1* sorghum genotype. Lignin+Si samples showed similar Si 2p spectra with higher signal to noise ratio (Fig. S2). Curves with filled area are deconvoluted peaks, the black line plus symbol curves represent the measured intensity, and the red curves represent the cumulative fit.

3.3 Identification of Si-O-C bonds and lignin potential to polymerize silicic acid

To study the chemistry between lignin and silica and to highlight possible Si-O-C bond formation, we reacted lignins with silicic acid solution (2.5, 5 mM) in phosphate buffer, herein lignin+Si. The solubility concentration of silicic acid in water is 1.7 mM [53], above which,

View Article Online
DOI: 10.1039/D5FD00011D

polymerisation to oligomeric silicic acid occurs. Therefore, we expected only minute amounts of silica polymerization. C 1s XPS spectra of lignin+Si precipitates demonstrated the reduction of C_3 (C=O, carbonyls) and the increase in C_2 (C-O, hydroxyls and ethers), compared to lignins that precipitated without silicic acid (Fig. 6ab, Table 3). This suggested that the surface carbonyl moieties on the lignin reacted with silicic acid to give Si-O-C bonds. High resolution Si 2p spectra of lignin+Si were similar to lignin samples before silicic acid addition, however, with increased signal to noise ratio (Fig. 6c, Fig. S2). Si-O-C bonds were detected in all samples, including lignin and lignin+Si, by the two major peaks at 102.1 eV (Si $2p_{3/2}$) and 102.7 eV (Si $2p_{1/2}$) (Fig. 6c), consistent with Si-O-C linkage [54]. In addition, two minor signals at 103.5 eV (Si $2p_{3/2}$) and 104.1 eV (Si $2p_{1/2}$) indicated Si-O-Si and Si-OH of silica (SiO_2) [55]. Our results suggest that with the addition of silicic acid, surface Si-O-C and Si-O-Si bonds increased by a similar factor, while Si-O-C occupied most of the C=O positions in Lig-LowSi, reducing surface carbonyls significantly.

FTIR spectra of lignin+Si in comparison to the corresponding lignin exhibited an interesting variation in the band at 469 cm^{-1}, assigned to Si-O-Si bending modes. Under reaction with marginally saturated silicic acid solution of 2.5 mM, lignin+Si spectra of only Lig-HighSi and not Lig-LowSi showed this peak. When silicic acid concentration was 5 mM it appeared in all lignin+Si samples, but its intensity was significantly higher in Lig-HighSi as compared to Lig-LowSi (Fig. 7). Further, pyrolysis residue during TGA of lignin+Si precipitates was found to be significantly higher in Lig-HighSi compared to Lig-LowSi (Fig. S3). Our results indicated that Lig-HighSi have a higher catalytic activity in polymerizing silicic acid. This could possibly occur through Si-phenoxyl bonds as Lig-HighSi contained higher free phenolics on the expense of β-O-4 linkages (Fig. 2,3) compared to Lig-LowSi [16].

Supporting this, lignin extracted using alkali pretreatment procedure in glass beakers showed a strong 469 cm^{-1} band only when extracted from BM-HighSi and not from BM-LowSi

(Supplementary Information SI2 and Fig. S4). This suggests that the Lig-HighSi could nucleate SiO_2 from silicic acid released from the glass beaker under alkaline pH, through binding silicic acid to the abundant phenolic hydroxyls and the formation of Si-phenoxyl bonds.

With addition of silicic acid, we detected an increase in a shoulder at 975 cm^{-1} and a band at 1240 cm^{-1}, exclusively assigned to Si-O-phenoxyl [47] (Fig. 7, Table 2). Further minor variations in the spectra could be attributed to Si-O-Si asymmetric stretching in cyclic siloxanes at 1015 cm^{-1}, open chain siloxanes at 1050 cm^{-1}, Si-O-C asymmetric stretching in ring-link at 1063 cm^{-1}, open-link Si-O-C at 1116 cm^{-1}, and cage-link Si-O-C asymmetric stretching modes at 1158 cm^{-1} [47,48].

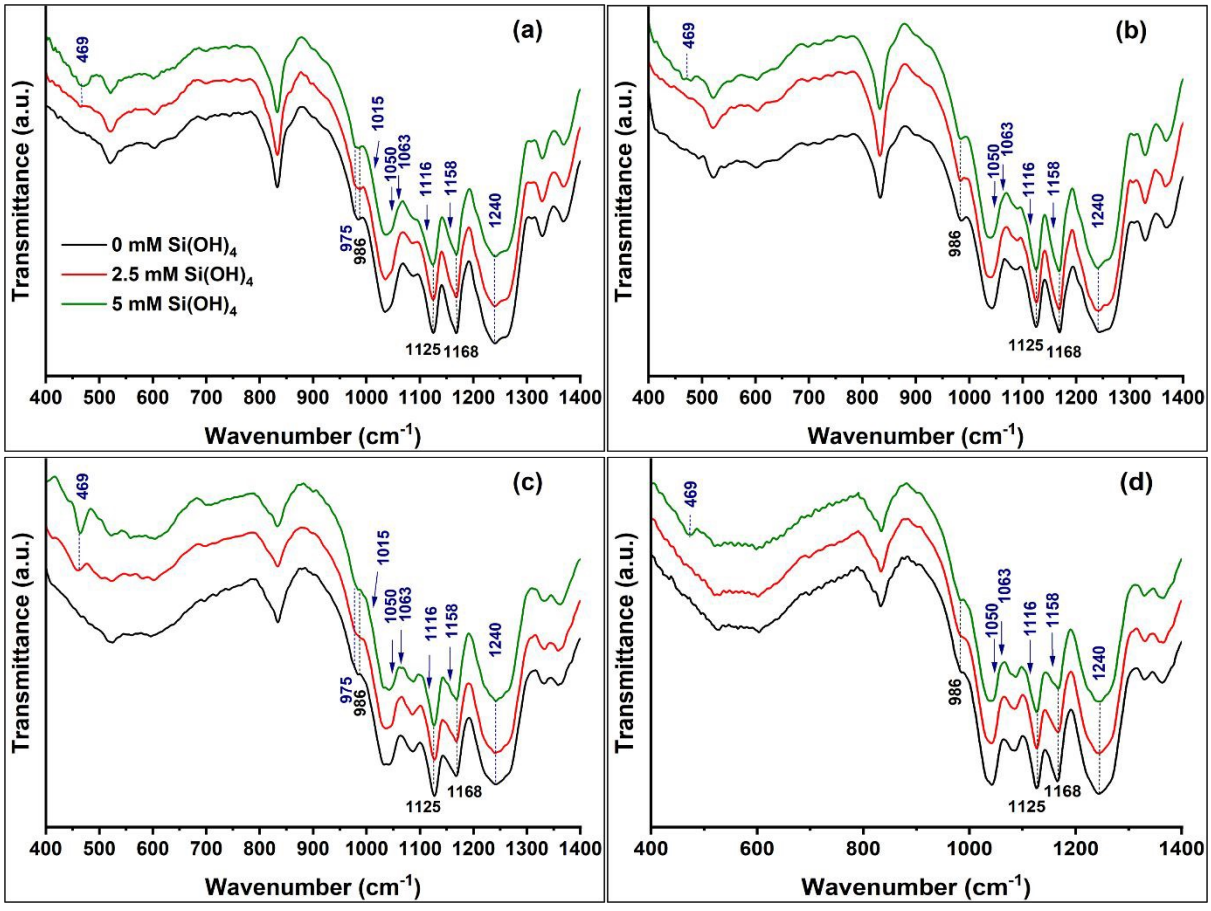

Figure 7: FTIR transmission spectra of lignin and lignin+Si precipitants. Lignins extracted from biomass of (a) WT, (b) *lsi1*, (c) *bmr6* and (d) *bmr6×lsi1* plants (black lines) were reacted with silicic acid at 2.5 mM (red) and 5 mM (green) to form lignin+Si precipitates. Peaks and

shoulder peaks of Si-O-Si and Si-O-C vibration modes are marked in blue text. Lignin major functional groups, marked in black text, overlapped with silica related peaks. Traces of Si-O-Si absorption band (469 cm^{-1}) appear when lignin reacted with 2.5 mM silicic acid only in WT and *bmr6*. This band is also strong in lignins extracted from biomass of WT and *bmr6* as compared to *lsi1* and *bmr6*×*lsi1* at 5 mM silicic acid.

In order to highlight these variations, we deconvoluted spectra of lignin and lignin+Si reacted with 2.5 mM silicic acid (Fig. 8). The area of the lignin bands at 1030 cm^{-1} assigned to C-O deformation of primary alcohols and methoxy groups, and at 1168 cm^{-1} assigned to conjugated C=O stretching, decreased with the addition of silicic acid, suggesting these bonds to react with silicic acid. Fitted peaks assigned to Si-O-C bonds at 975, 1240, 1116 and 1158 cm^{-1}, and Si-O-Si bonds at 1050 cm^{-1} were observed in the spectra of all samples, and their relative integrated absorption area increased in lignin+Si precipitates. Two very small peaks, attributed to Si-O-Si asymmetric cyclic siloxanes stretching (1015 cm^{-1}), and Si-O-C ring-link modes (1063 cm^{-1}) could be fitted only in the spectra of lignin+Si precipitates.

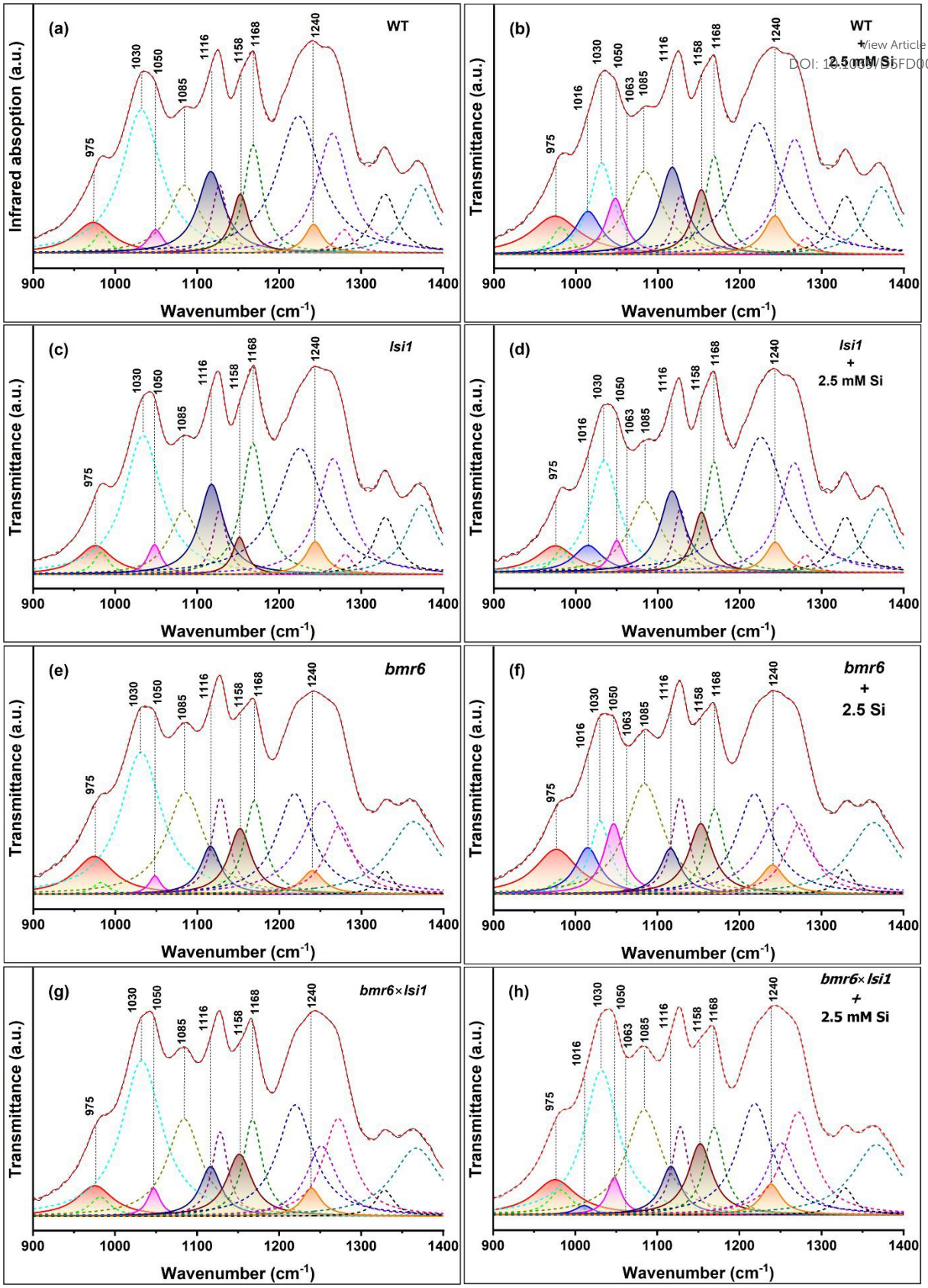

Figure 8: Deconvolution of FTIR spectra of extracted lignin and lignin+Si reacted with 2.5 mM silicic acid. Si-O-C and Si-O-Si bonding modes are highlighted in the wavenumber

View Article Online
DOI: 10.1039/D5FD00011D

range from 950 to 1250 cm^{-1}. Spectra of lignin extracted from biomass of (a) WT, (c) *lsi1*, (e) *bmr6*, and (g) *bmr6×lsi1* plants were compared to lignin+Si precipitates of (b) WT, (d) *lsi1*, (f) *bmr6*, and (h) *bmr6×lsi1* plants. Black line represents infrared absorption, and red dashed line represents the cumulative peak fit of lignin (coloured-dashed lines) and Si-O (full lines with filled area).

Based on the fit, we calculated the difference between the intensities of selected bands in lignin+Si and lignin samples (Fig. 9). As expected by our previous analysis (Fig. 7), with silicic acid addition, the increment in the integrated absorption area of the bands at 975 and 1240 cm^{-1} assigned to Si-O-phenoxyl bonding was higher in Lig-HighSi compared to Lig-LowSi (Fig. 9a). Furthermore, the relative increase in the integrated absorption area of Si-O-Si asymmetric stretching in cyclic siloxanes (at 1016 cm^{-1}) and open chain siloxanes (at 1050 cm^{-1}) was greater in Lig-HighSi compared to Lig-LowSi (Fig. 9b).

Peaks related to the open-link Si-O-C bonds at 1116 cm^{-1} and cage-link Si-O-C bonds at 1158 cm^{-1} increased with addition of silicic acid more in Lig-LowSi compared to Lig-HighSi (Fig 9c). In parallel, a similar decrement was observed in the relative absorption of conjugated C=O stretching at 1168 cm^{-1}, and less so in C-O deformations at 1030 cm^{-1} (Fig 9d). Taking into account the XPS results (Fig. 6a,b), the higher formation rate of Si-O-C with Lig-LowSi could be due to the availability of surface carbonyl groups to readily react with silicic acid and form Si-O-C bonds.

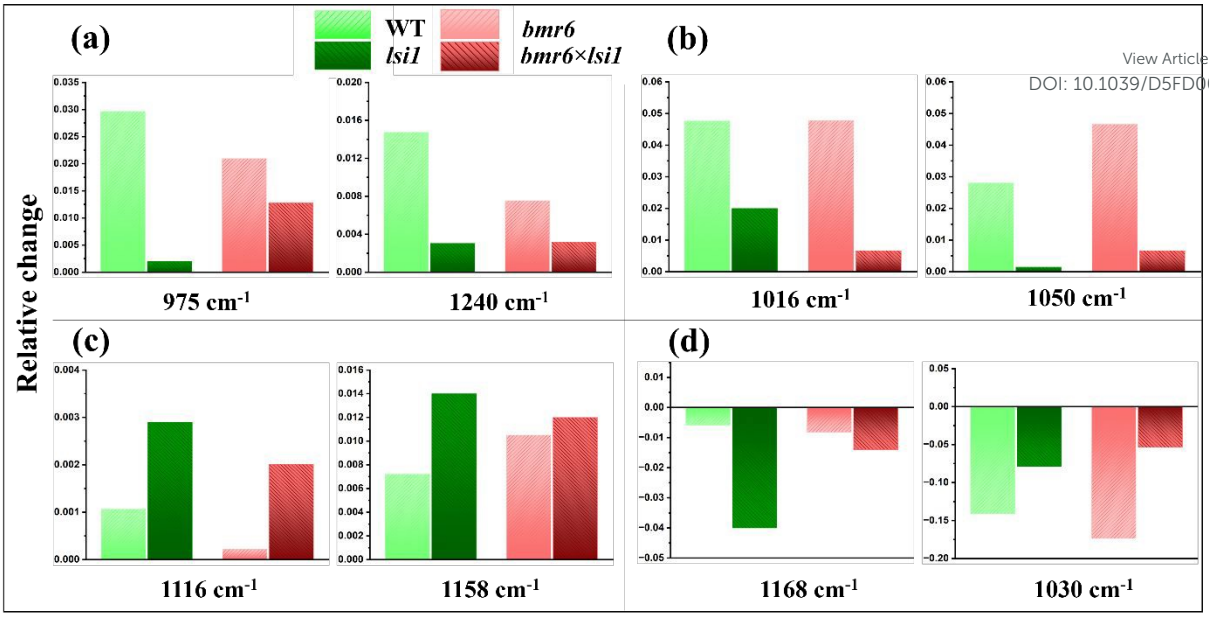

Figure 9: Relative changes in the integrated absorption of lignin functional groups and Si-O-Si and Si-O-C modes in lignins from the different sorghum genotype as a result of reaction with silicic acid. (a) Changes in bands at 975 and 1240 cm^{-1} assigned to the Si-O-C bonding modes in which Si is bonded to the phenoxyl group. (b) Changes in bands at 1016 cm^{-1}, assigned to Si-O-Si cyclic siloxanes, and at 1050 cm^{-1}, assigned Si-O-Si open chain siloxanes. (c) Changes in bands at 1116 and 1158 cm^{-1} assigned to open-link and cage-link Si-O-C bonds respectively. (d) Bands at 1168 cm^{-1}, assigned to conjugated C=O, and at 1030 cm^{-1}, assigned to C-O deformation in primary alcohols and methoxy groups, reduced with addition of silicic acid.

3.4 Silica nanoparticles distribution in lignin of high-silicon genotype

Tomography by scanning electron transmission microscopy (STEM) was performed in order to examine the distribution of silica within the agglomeration of lignin particles. Specimens were prepared using lignin extracted from *bmr6* and *bmr6×lsi1* plants, both exposed to silicic acid solution of 2.5 mM concentration. Figure 10 shows 60 nm thick virtual sections from the top, middle, and bottom of the specimens in a semi-transparent volume display mode. (In

View Article Online
DOI: 10.1039/D5FD00011D

addition, depth sectioning movies are provided in the supplementary information: video clips S1 and S2). The two specimens appear as similar agglomerates of near-spherical particles some tens of nm in diameter forming a film of overall thickness 300-350 nm. Particles are clearly visible at the top and bottom of the clusters. They appear to have fused together near the central plane, but this may reflect a loss of resolution for boundaries and small channels within the bulk of the material. Notably, small dense particles of about 6-10 nm diameter appear near the mid-section of the *bmr6* specimen, but are absent in the *bmr6×lsi1*. Given the evidence from SEM-EDS, indicating a Si:C ratio of 3%, the small particles would not appear to account for all the silicon. Other silicon fractions could be bound as single or oligomeric silicic acid units dispersed within the lignin matrix. In order to investigate this, the same grids used for tomography were examined by the more sensitive STEM-EDS. A significant concentration of Si was found in the *bmr6* specimen, distributed throughout the lignin. Si was detected in the *bmr6×lsi1* specimen only at a level very close to background. These results establish strong evidence that lignin of the high silicon genotype, which has fewer β-O-4 linkages and free phenolics, effectively catalyse silicic acid to incorporate silica within the lignin matrix.

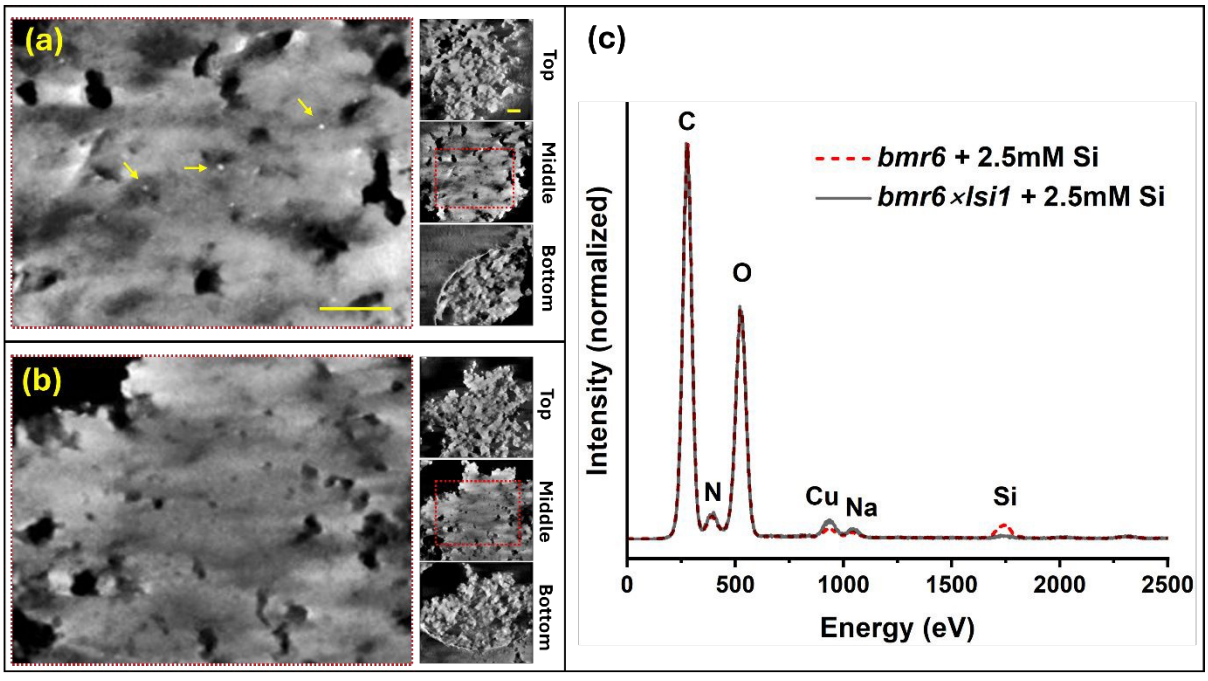

View Article Online
DOI: 10.1039/D5FD00011D

Figure 10: Electron tomography of agglomerates of lignin extracted from *bmr6* and *bmr6×lsi1* plants, exposed to silicic acid at a concentration of 2.5 mM. (a) Thick virtual section reconstructed from the mid-plane of the *bmr6* specimen; note the dense nanoparticles indicated by yellow arrows, which we identify as silica deposits due to the strong electron scattering. Insets to the right show the top, middle, and bottom sections to indicate the texture of small, clustered particles of lignin at top and bottom. The bright circular arc in the bottom section is the edge of a hole (2 um diameter) in the specimen support film. (b) Virtual sections of the *bmr6×lsi1* specimen, organized as above. Bright nanoparticles were not observed. Scale bar in panel a is 200 nm, common to a and b. Scale bar in the top inset is 200 nm, common to all insets. (c) EDX spectra recorded from the same grids, showing the higher concentration of Si in the lignin extracted from the *bmr6* plant than from the *bmr6×lsi1*.

4. Conclusion

The presented results indicated that Si-O-C bonds form primarily on lignin phenolic hydroxyls and conjugated carbonyl moieties either in the plant or during extraction. Lignin extracted from biomass of plants with native-silicon intake showed a higher catalytic activity, polymerizing SiO_2 with higher content of Si-phenoxyl bonds, as compared to SiO_2 forming on lignin of low-silicon mutants. In synthetic lignin, the presence of phenoxy radicals and/or quinone methides of short lignin fragments have high affinity towards silica, and form cyclic siloxanes with Si-phenoxyl bonds instead of extended Si-O-Si network [16]. The low content of β-O-4 ether linkages between monolignol units and high content of Si-O-Si formation with Lig-HighSi suggest that free phenolics (O-4) catalyse silicic acid condensation. In the *bmr6* genotype we measured higher SiO_2 content as compared to the WT genotype (Table 1 and Fig. 7, in agreement with our published data [15]. This could be explained by the increase in aliphatic

carbonyl moieties forming under *bmr6* mutation, which enhance the catalytic activity of lignin in silicic acid condensation.

View Article Online
DOI: 10.1039/D5FD00011D

Interestingly, lignin and silica are not colocalized in the plant. Most lignin is polymerized in the vascular bundles, in xylem tracheary elements and fibre cells. In contrast, most silica is deposited at the epidermis, in silica cells and hairs and forming a double layer with the cuticle. Nonetheless, our work indicates significant variations in the lignin structure as a result of silicic acid intake. The presented data indicate that silicic acid, when present in the apoplast, affects the radical dehydrogenation and polymerization of monolignols by capping the O-4 phenoxyl position. These positions are available in the polymerized lignin for H-bonding to other polymers and molecules and for binding cations. Such variations may explain some of the beneficial effects of silica in plants exposed to heavy metals [56].

The presence of silicic acid during *in vivo* lignin polymerization apparently leads to the aryl-silyl ether (Si-O-4) bonds between silicic acid and monolignol phenoxyl radicals/quinone methides. This may lead to abundant phenoxyl Si-O-C bonds that effectively catalyse the polymerization of silicic acid into SiO_2 nano particles. In contrast, Lig-LowSi may be produced with abundant aryl-alkyl ether (β-O-4) bonds between monomers that would increase the cell wall density and the extension of conjugated carbonyls. This could explain the appearance of dense lignified cell walls with red-shifted autofluorescence in roots grown under low silicon conditions [37]. The common paradigm asserts that silica reduces biomass digestibility in parallel to lignin [57,58]. This work highlights a more complex relationship between the two materials as silica actually changes lignin, and *vice versa*. Extending this research will show whether the modified lignin has implication on the biological function of the tissue and valorisation of biomass.

View Article Online
DOI: 10.1039/D5FD00011D

Conflicts of interest:

There are no conflicts to declare.

Data availability:

The STEM and STEM-EDX data that support the findings of this study are available under doi:10.5281/zenodo.14686717.

Acknowledgements:

We thank Nerya Zexer for producing double mutant plants by crossing between *bmr6* and *lsi1* sorghum plants, Shula Blum for isolating the homozygote *bmr6×lsi1* plants, and Lothar Houben for assistance with STEM-EDS. S.P. is thankful for a scholarship from Lady Davis and Golda Meir. This work was funded in part by the Israel Science Foundation grant 958/21. Contribution of ME was supported by the European Union (ERC, CryoSTEM, 101055413; Views and opinions expressed are however those of the authors only and do not necessarily reflect those of the European Union or the European Research Council. Neither the European Union nor the granting authority can be held responsible for them.) ME is incumbent of the Sam and Ayala Zacks Professorial Chair in Chemistry.

Supporting information:

Production and isolation of a sorghum line carrying both *bmr6* and *lsi1* mutations (Supporting Information, SI1), Lignin extracted using alkali pretreatment process (Supporting Information, SI2), A representative GC-MS chromatogram of trimethyl-silyl (TMS) derivatives of sorghum genotype thioacidolysis products (Figure S1), High resolution XPS Si 2p spectra of lignin+Si from WT, *lsi1*, *bmr6* and *bmr6×lsi1* sorghum genotype at silicic acid concentration of 2.5 mM (Figure S2), Thermal decomposition behaviour of lignins reacted with different concentrations of silicic acid in phosphate buffer solution (Figure S3), FTIR transmission spectra of lignin

extracted using alkali pretreatment process (Figure S4), Tomographic sections of the high silicon specimen (*bmr6* + 2.5 mM Si), scale 1.5 nm/pixel (Movie 1), Tomographic sections of the low silicon specimen (*bmr6*×*lsi1* + 2.5 mM Si), scale 1.5 nm/pixel (Movie 2).

References

View Article Online
DOI: 10.1039/D5FD00011D

1 L. A. Estroff, Introduction: Biomineralization, *Chem Rev*, 2008, **108**, 4329–4331.

2 R. Wood, Exploring the drivers of early biomineralization, *Emerg Top Life Sci*, 2018, **2,** 201–212.

3 P. U. P. A. Gilbert, K. D. Bergmann, N. Boekelheide, S. Tambutté, T. Mass, F. Marin, J. F. Adkins, J. Erez, B. Gilbert, V. Knutson, M. Cantine, J. Ortega Hernández and A. H. Knoll, Biomineralization: Integrating mechanism and evolutionary history, *Sci Adv*, 2022, **8**, 1-16.

4 N. Mitani-Ueno, N. Yamaji, S. Huang, Y. Yoshioka, T. Miyaji and J. F. Ma, *Nat Commun*, 2023, **14**, 6522.

5 S. Kumar, M. Soukup and R. Elbaum, *Front Plant Sci*, 2017, **8**, 438.

6 N. Zexer, S. Kumar and R. Elbaum, *Ann Bot*, 2023, **131,** 897–908.

7 Z. Lukačová, R. Švubová, J. Kohanová and A. Lux, *Plant Growth Regul,* 2013, **70**, 89–103.

8 A. T. Fleck, T. Nye, C. Repenning, F. Stahl, M. Zahn and M. K. Schenk, *J Exp Bot*, 2011, **62**, 2001–2011.

9 R. R. Rivai, K. Yamazaki, M. Kobayashi, Y. Tobimatsu, T. Tokunaga, T. Fujiwara and T. Umezawa, *Plant Cell Physiol*, 2024, **65**, 1983–1992.

10 K. Radotić, D. Djikanović, A. Kalauzi, G. Tanasijević, V. Maksimović and J. Dragišić Maksimović, *Int J Biol Macromol*, 2022, **198**, 168–174.

11 Fang, J., Wang, H., Chen, Y., & Zhang, F., *Prog. Nat. Sc*, 2003, **13**, 501-504.

12 J. yu Fang and X. long Ma, *J Zhejiang Univ Sci B*, 2006, **7**, 267–271.

13 M. Soukup, V. M. Rodriguez Zancajo, J. Kneipp and R. Elbaum, *J Exp Bot*, 2020, **71**, 6807–6817.

14 C. Zhang, L. Wang, W. Zhang and F. Zhang, *Plant Soil*, 2013, **372**, 137–149.

15 N. Zexer and R. Elbaum, *J Exp Bot*, 2022, **73**, 1450–1463.

16 S. Palakurthy, L. Houben, M. Elbaum and R. Elbaum, *Biomacromolecules*, 2024, **25**, 3409-3419.

17 D. Delmer, R. A. Dixon, K. Keegstra and D. Mohnen, *Plant Cell*, 2024, **36**, 1257–1311.

18 J. H. Coomey, R. Sibout and S. P. Hazen, *New Phytologist*, 2020, **227**, 1649–1667.

19 L. Salmén, *Cellulose*, 2022, **29**, 1349–1355.

20 J. Gierer, *Wood Sci. Technol*, 1985, **19**, 289-312.

21 J. Snelders, E. Dornez, B. Benjelloun-Mlayah, W. J. J. Huijgen, P. J. de Wild, R. J. A. Gosselink, J. Gerritsma and C. M. Courtin, *Bioresour Technol*, 2014, **156**, 275–282.

22 H. Labauze, N. Cachet and B. Benjelloun-Mlayah, *Ind Crops Prod*, 2022, **187**, 115328.

23 F. Abdelkafi, H. Ammar, B. Rousseau, M. Tessier, R. El Gharbi and A. Fradet, *Biomacromolecules*, 2011, **12**, 3895–3902.

24 Q. Zheng, L. Chai, B. Du, W. Li, L. H. Fu and X. Chen, *Polymers (Basel)*, 2023, **158**, 1867.

25 I. Tari, G. Laskay, Z. Takács and P. Poór, *J Agron Crop Sci*, 2013, **199**, 264–274.

26 S. Głazowska, L. Baldwin, J. Mravec, C. Bukh, T. H. Hansen, M. M. Jensen, J. U. Fangel, W. G. T. Willats, M. Glasius, C. Felby and J. K. Schjoerring, *Biotechnol Biofuels*, 2018, **11**:171, 1-18.

27 W. L. Rooney, J. Blumenthal, B. Bean and J. E. Mullet, *Biofuel Bioprod Biorefin*, 2007, **1**, 147–157.

28 A. G. Sangster and D. W. Parry, *Ann. Bot*, 1976, **40**, 361-371.

29 O. Markovich, S. Kumar, D. Cohen, S. Addadi, E. Fridman and R. Elbaum, *Silicon*, 2019, **11**, 2385–2391.

30 E. D. Scully, T. Gries, D. L. Funnell-Harris, Z. Xin, F. A. Kovacs, W. Vermerris and S. E. Sattler, *J Integr Plant Biol*, 2016, **58**, 136–149.

31 J. D. Gargulak, S. E. Lebo and T. J. McNally, *Kirk-Othmer Encyclopedia of Chemical Technology*, Wiley, 2015, 1–26.

32 Z. Peleg, Y. Saranga, T. Fahima, A. Aharoni and R. Elbaum, *Physiol Plant*, 2010, **140**, 10–20.

33 A. E. Harman-Ware, C. Foster, R. M. Happs, C. Doeppke, K. Meunier, J. Gehan, F. Yue, F. Lu and M. F. Davis, *Biotechnol J*, 2016, **11**, 1268–1273.

34 S. Seifer, L. Houben and M. Elbaum, *Microscopy and Microanalysis*, 2021, **27**, 1476–1487.

35 D. N. Mastronarde and S. R. Held, *J Struct Biol*, 2017, **197**, 102–113.

36 T. Emiola-Sadiq, L. Zhang and A. K. Dalai, *ACS Omega*, 2021, **6**, 22233–22247.

37 N. Zexer and R. Elbaum, *J Exp Bot*, 2020, **71**, 6818-6829.

38 J. Ralph, J. H. Grabber, *Holzforschung*, 1996, **50**, 425-428.

39 C. Lapierre, B. Pollet, B. Monties and C. Rolando, *Holzforschung*, 1991, **45**, 61-68.

40 T. Faravelli, A. Frassoldati, G. Migliavacca and E. Ranzi, *Biomass Bioenergy*, 2010, **34**, 290–301.

41 X. Lu and X. Gu, *Biotechnol Biofuels*, 2022, **15**, 106.

42 S. E. Sattler, D. L. Funnell-Harris and J. F. Pedersen, *J Agric Food Chem*, 2010, **58**, 3611–3616.

43 H. L. Hergert and E. F. Kurth, *J. Org. Chem*, 1953, **18**, 521-529.

44 T. You and F. Xu, Applications of Molecular Spectroscopy to Current Research in the Chemical and Biological Sciences, *InTech*, 2016, 235-260, https://doi.org/10.5772/64581.

45 R. J. Sammons, D. P. Harper, N. Labbé, J. J. Bozell, T. Elder and T. G. Rials, *Bioresources*, 2013, **8**, 2752–2767.

46 P. Bock, P. Nousiainen, T. Elder, M. Blaukopf, H. Amer, R. Zirbs, A. Potthast and N. Gierlinger, *Journal of Raman Spectroscopy*, 2020, **51**, 422–431.

47 *B*ellamy, L. J. The Infra-Red Spectra of Complex Molecules; Chapman and Hall: London, 1975, 374– 384.

48 G. L. L. Barry Arkles, *Silicon Compounds- Silanes and Silicones*, Gelest: Morrisville, USA, 3rd edn., 2013.

49 R. Al-Oweini and H. El-Rassy, *J Mol Struct*, 2009, **919**, 140–145.

50 J. Wang, K. Yao, A. L. Korich, S. Li, S. Ma, H. J. Ploehn, P. M. Iovine, C. Wang, F. Chu and C. Tang, *J Polym Sci A Polym Chem*, 2011, **49**, 3728–3738.

51 C. M. Popescu, C. M. Tibirna and C. Vasile, *Appl Surf Sci*, 2009, **256**, 1355–1360.

52 M. Ragnar, C. T. Lindgren and N. O. Nilvebrant, *J. Wood Chem. Technol*, 2000, **20**, 277–305.

53 R. K. Iler, The chemistry of silica : solubility, polymerization, colloid and surface properties, and biochemistry, Wiley, New York, 7th edition., 1979.

54 A. Avila, I. Montero, L. Galán, J. M. Ripalda and R. Levy, *J Appl Phys*, 2001, **89**, 212–216.

55 G. Dakroub, T. Duguet, J. Esvan, C. Lacaze-Dufaure, S. Roualdes and V. Rouessac, *Surf. Interfaces*, 2021, **25**, 101256.

56 B. Bokor, C. S. Santos, D. Kostoláni, J. Machado, M. N. da Silva, S. M. P. Carvalho, M. Vaculík and M. W. Vasconcelos, *J Hazard Mater*, 2021, **416**, 126193.

57 P. J. Van Soest and L. H. P. Jones, *J Dairy Sci*, 1968, **51**, 1644–1648.

58 M. P. Silva, C. Whitehead, R. L. Ordonio, T. C. Fernando, M. P. B. Castillo, J. L. Ordonio, T. Larson, D. J. Upton, S. E. Hartley and L. D. Gomez, *Biomass Bioenergy*, 2024, **182**, 107099.

Data availability:

View Article Online
DOI: 10.1039/D5FD00011D

The STEM and STEM-EDX data that support the findings of this study are available under doi:10.5281/zenodo.14686717.